# Myopia



**Right eye**

**Left eye**

**TECHNICAL REPORT**

**The effects of severe myopia on**

**the properties of sampling units in peripheral retina**

by

Manbir Nagra[1] PhD, Bernard Gilmartin[2] PhD, DSc,

Nicola S Logan[2] PhD and Stephen J Anderson[2]* PhD

[1]Centre for Applied Vision Research, City, University of London, EC1V 0HB, UK

[2]School of Life and Health Sciences, Aston University, Birmingham B4 7ET, UK

**Keywords:** Myopia, Peripheral vision, Ganglion cell density, Ocular shape, Refractive development, Aliasing

**Word Count**: 2996 (excluding references and figure legends)

**Figures**: 3

**\*Corresponding author**: Prof. S.J. Anderson (email: s.j.anderson@aston.ac.uk)

## ABSTRACT

***Significance:*** Poor peripheral visual acuity in myopia may reflect, in part, photoreceptor misalignment with the exit pupil of the eye. We speculate that if such misalignment causes sufficient visual deprivation and/or disrupts retinal feedback processes, it may influence eye growth itself.

***Purpose:*** It is known that myopic eyes have a reduced peripheral resolution acuity relative to emmetropic eyes, though it remains unclear how mechanical stretching of the retina in myopia impacts on peripheral visual performance. Our aim was to determine how retinal stretching affects the properties of sampling units in peripheral vision.

***Methods:*** Three-dimensional magnetic resonance imaging provided a depiction *in vivo* of ocular shape, allowing the inter-eye ratio of retinal image surface areas and the relative alignment of surfaces to be determined in our observer, who was unique in having severe myopia in the right eye (~21D) but only modest myopia in the left (~3D). Visual performance was assessed for the detection and direction discrimination of drifting sinusoids positioned 40⁰ in the temporal retina. Applying the sampling theorem to our measures, we estimated the density and cut-off frequency of the underlying sampling units.

***Results:*** The retinal image surface area of the right eye was 40% larger than that of the left, and was rotated 8.9⁰ anticlockwise relative to the left eye's image surface. In agreement with a linear stretch model of myopia, the sampling density of the right eye was reduced by approximately the same ratio as that predicted from the inter-eye MRI data, namely 1.18. However, the cut-off frequency (cycles/mm) of the right eye was approximately half that of the left, a reduction that cannot be explained solely by a linear areal expansion of retinal sampling units.

***Conclusions:*** Poor peripheral acuity in severe myopia may be caused, at least in part, by receptoral misalignment with the exit pupil.

1   Although the central spatial acuity of corrected myopes is similar to that of emmetropes,[1,2]

2 various reports suggest that the peripheral acuity of myopes is reduced relative to emmetropes.[1-

3 3] Reasons for this reduced acuity remain unclear, though candidate properties of the myopic retina

4 that may underlie this finding include the size, density and spatial arrangement of ganglion cells

5 and/or photoreceptors. It is well known, for example, that spatial acuity declines with distance

6 from the fovea at a faster rate than that dictated by the optical properties of the human eye, with

7 several reports suggesting that peripheral acuity is principally determined by the receptive field

8 size and sampling density of ganglion cells.[4-8]  With excessive expansion of the posterior vitreous

9 chamber, as occurs in severe myopia,[9-11] sampling density may be decreased[1-3] and

10 photoreceptors may be misaligned with the exit pupil.[12,13]

11   Our principal aim was to determine how retinal stretching from severe myopia affects the

12 properties of sampling units in human peripheral retina. We used three-dimensional magnetic

13 resonance imaging to depict ocular shape, while sampling density was measured *in situ* by

14 making use of the fact that human peripheral vision is susceptible to anomalous motion perception

15 because of spatial aliasing.[7,14-16] The frequency at which aliasing first occurs is indicative of the

16 Nyquist limit of the underlying sampling mosaic,[17,18] which is known to be the parvocellular

17 ganglion cell matrix in the far temporal retina.[7,15] Following the example of these aliasing studies,

18 we assessed the effects of severe myopia on visual performance for both the direction

19 discrimination and detection of drifting sinusoids positioned at 40º in the temporal retina. From

20 these measures, employing the sampling theorem, we determined the density and filtering

21 properties of the underlying sampling matrix. A simple linear stretch model of myopia predicts a

22 decrease in sampling density with a concomitant increase in spatial pooling by the sampling units.

23   As our highly anisomyopic (~ 18 D) observer was distinguished by having only a modest

24 level of myopia in his 'good eye', we employed the same observer for both experimental and

25 control measures.

26

## METHODS

28     The study was approved by the Aston University Research and Ethics committee and

29     complied with the 1964 Helsinki Declaration and its later amendments. Informed written consent

30     was obtained from the subject in this study. Identifying subject features have been removed to

31     ensure anonymity.

32

### Refractive details of observer

34     The observer was a 45 year old male anisomyope. His central refractive errors, as

35     measured using streak retinoscopy, were: right eye (RE) = -19.75/-1.50 x 95; left eye (LE) = -

36     2.25/-1.00 x 27.  His spectacle-corrected central visual acuities were:  RE, 6/6 (logMAR 0.00); LE,

37     6/5 (logMAR -0.08).  Central Mean Spherical Error (MSE) was -20.50D in the right eye and -2.75D

38     in the left eye, producing 17.75D of central anisometropia. At age 10 years, the observer's

39     refractive error was approximately -7.00D RE and -1.00D LE, indicating that most of the refractive

40     changes in his right eye occurred late into (or after) the critical period of visual development. The

41     observer, a qualified optometrist, reported that his central refractive error was stable from 16-17

42     years of age. The spectacle refractive error at $40^0$ temporal to the fovea, determined using streak

43     retinoscopy, was -8.00/-2.50 x 90 for the right eye and -3.50/-1.50 x 90 for the left.  Peripheral

44     refractive error was corrected using full aperture trial lenses at a vertex distance of 12 mm.

45

### Determination of surface area

47     Magnetic resonance (MR) images were obtained for the right and left eyes of the observer

48     using procedures initially reported by Singh et al.,[19] and recently used to measure posterior

49     vitreous chamber shape in both myopia and emmetropia.[20-22] In brief, the observer was scanned

50     using a Siemens Trio 3-tesla MRI scanner with an 8-channel phased-array head-coil. A T-2

51    weighted scan was used to demarcate fluid-based intraocular structures for each eye, providing

52    a high-contrast delineation of the vitreous-retina interface.

53         Following Gilmartin et al.,[20] the 3D co-ordinates for nasal and temporal quadrants for each

54    eye were collapsed and superimposed about the nasal-temporal meridian and plotted in two

55    dimensions as distance-along and distance-from the visual axis for 15% to 100% of eye length.

56    Whereas Gilmartin et al. plotted the mean distance from the visual axis against the midpoint of

57    successive percentage intervals of axial length, the present study employed a 10-point moving

58    average of MRI data to represent ocular shape (Fig. 1A).

59         The second nodal point (NP2) was adopted as a pivotal reference point for the

60    representation of ocular shape. NP2, which was assumed to be located at the posterior pole of

61    the crystalline lens, bisects the line representing distances from NP2 to the two adjacent vitreous-

62    retina interfaces;[20] the axis orthogonal to this line is coincident with the visual axis. The distance

63    from the posterior pole of the cornea to NP2 for the RE and LE (7.7 mm and 7.5 mm, respectively)

64    was taken as the sum of the anterior chamber depth (3.5 mm and 3.3 mm, respectively) and lens

65    thickness (4.2 mm). The latter was calculated from the regression equation for age versus lens

66    thickness,[23] which was considered appropriate as recent studies show no significant relationship

67    between refractive error and lens thickness.[24]

68         The position of NP2 was used to locate, by projection, the regions of the temporal retinae

69    conjugate with the 40º nasal location of the stimulus display. As the difference in positions of NP2

70    for the RE and LE was small (0.2 mm), for expediency single lines were drawn at 40º in Fig. 1A

71    and 40º ±3º in Fig. 1B to represent, for both eyes, the 6º angular subtense of the stimulus display.

72         BC and FG (mm) in Fig. 1B indicate the distances projected onto the temporal retinae of

73    the right and left eye, respectively, by the stimulus display. Constituent distances AB and AC were

74    calculated by application of Pythagoras' theorem to triangles ABE and ACD, respectively

75    (distances AE, BE and AD, CD were available from x- and y-co-ordinates of the MRI data output).

76    The distance between B and C (F and G) was assumed to be linear and calculated by applying

77   the Cosine Rule to triangle ABC (AGF). The right and left eye retinal surface areas corresponding

78   to the square stimulus display were therefore $BC^2$ and $FG^2$, respectively.

79

80   **Measures of detection and direction discrimination performance**

81   *Stimuli.* All stimuli were generated using a VSG2/5 graphics board (from Cambridge Research

82   Systems) and displayed on a Sony FD Trinitron monitor with 14-bit luminance resolution at a non-

83   interlaced frame rate of 100 Hz. The stimulus was a horizontally-oriented sinusoidal grating of

84   spatial frequency 1.0 – 6.0 cycles/deg, drifting either up or down at a temporal frequency of 8 Hz.

85   The grating had a Michelson contrast of 0.8, and was presented within a $6^o$ square patch at a

86   viewing distance of 1 m. The sharp edges of the patch were attenuated with a cosine ramp of

87   $0.75^o$ width. The mean luminance of the display was 40 cd/$m^2$.

88

89   *Procedure.* The display was viewed monocularly at an eccentricity of $40^o$ (temporal retina). The

90   fixation target was a red light emitting diode, with eccentricity measured from the centre of the

91   stimulus.

92        A two-interval forced-choice procedure was used in conjunction with method of constant

93   stimuli to measure psychometric functions relating performance for both detection and direction

94   discrimination criteria to stimulus spatial frequency. For detection, one interval contained a

95   sinewave grating that drifted either upwards or downwards with equal probability, while the other

96   contained a blank field of the same mean luminance. The task of the observer was to indicate

97   (using a button press) which interval contained the grating. For direction discrimination, one

98   interval contained an upward-drifting grating and the other, a downward-drifting grating. The task

99   of the observer was to indicate which interval contained the upward-drifting grating. For both

100  criteria, the intervals were presented in random order, lasted 1 s each, and were separated by a

101  blank screen of 1 s duration. Each datum was calculated as the percentage of correct responses

102  from a minimum of 25 trials. No feedback was given. To minimize both Troxler's effect and local

103  adaptation effects, the observer was instructed to close his eyes for 30 s after every 10 trials.

104

105  **RESULTS AND DISCUSSION**

106  **Retinal surface area and rotation**

107  Stimulus display surface areas for the temporal quadrants of the right and left eyes, based

108  on the MRI surface area data (Fig. 1), were calculated to be 3.36 mm$^2$ (BC$^2$) and 2.40 mm$^2$ (FG$^2$),

109  respectively. The retinal image size in the highly myopic right eye was therefore 40% larger than

110  the image size in the mildly myopic left eye (ratio 1.4).

111  With a simple linear expansion of the globe, spatial acuity in angular units (cycles/deg) for

112  both direction discrimination and detection should remain unchanged because the increased

113  optical image size would compensate for any changes in the density and size of the retinal

114  sampling units. In order to demonstrate the effects of severe myopia on the anatomical properties

115  of retinal units, therefore, we plotted our psychophysical data in linear units on the retina

116  (cycles/mm) rather than angular units. With this approach, and assuming a linear stretch model

117  of myopia and a regular sampling matrix, both the sampling density and cut-off spatial frequency

118  (in cycles/mm) of the underlying units will vary in inverse proportion to the extent of retinal

119  stretching. Based on our MRI surface area data (Fig. 1), the sampling density and cut-off

120  frequency of the right eye should be less than that of the left eye (along a single dimension) by a

121  factor of 1.18 (i.e. $\sqrt{1.4}$).

122  From Fig. 1B, sine DE/BC determined the angle retinal surface BC makes with the

123  horizontal (55.3º). The angle for surface FG was similarly calculated (46.4º), indicating that the

124  retinal surface in the RE was rotated 8.9º anticlockwise relative to the LE.

125

126  **Detection performance**

127    Figure 2 shows the performance (percentage of correct responses) of the observer for the

128    criterion of detection, plotted as a function of stimulus periodicity. Performance declined to chance

129    (50% correct) with increasing stimulus spatial frequency for both right- (filled circles) and left-eye

130    (open circles) viewing. The curve through each data set shows the least-squares fit of a Weibull

131    function. With threshold defined at the 80% correct level, the measured spatial acuity was 16.46

132    cycles/mm for the left eye and 7.78 cycles/mm for the right eye. Note that the predicted acuity of

133    the right eye, based on the inter-eye MRI surface area data, was 13.95 cycles/mm (i.e.

134    16.46/1.18).

135    Converting the psychophysical data to angular units, the measured spatial acuity was 2.38

136    cycles/deg for the right eye, which is 44% less than the measured acuity of 4.25 cycles/deg for

137    the left eye. This difference in spatial acuity is incompatible with a simple linear stretch model of

138    myopia. Note that the acuity of the left eye (4.25 cycles/deg) closely approximates the receptive

139    field cut-off frequency of parvocellular ganglion cells at 40° eccentricity in individuals with little or

140    no ametropia.[7]

141

142    **Direction discrimination performance**

143    The psychometric functions for direction discrimination, shown in Fig. 3, differ both

144    quantitatively and qualitatively to those for detection. Performance for direction discrimination fell

145    to chance level at 9.50 cycles/mm for the left eye (open circles) and 7.75 cycles/mm for the right

146    eye (closed circles), and did so for each eye despite detection performance exceeding 80%

147    correct (see Fig. 2). For the highly myopic right eye, performance remained near chance for higher

148    stimulus periodicities. For the left eye, however, performance continued to decline below chance

149    with increasing stimulus spatial frequency, reaching zero percent correct at 10.7 cycles/mm

150    before rising to chance again near 13.5 cycles/mm. This decline in performance below chance

151    indicates that the grating stimulus was perceived drifting in the wrong direction, which is consistent

152    with it having been spatially undersampled.[4,7,14,15]

153    The sampling theorem predicts that, with drifting gratings and a regular sampling matrix,

154    direction discrimination performance should be at chance for periodicities matching the Nyquist

155    limit of the matrix because the stimulus will alias to a counterphased grating at that limit; grating

156    periodicities greater than the Nyquist limit but less than twice the Nyquist limit will alias to a grating

157    drifting in the opposite direction to the input grating.[17] Given this, we estimate the sampling density

158    of the underlying mosaic to be 9.50 cycles/mm (from Fig 3) for the mildly myopic left eye, a value

159    which is in accord with previous estimates of ganglion cell density, at 40⁰ in the temporal retina of

160    normally-sighted observers.[7,15,18]

161    Assuming a linear stretch model of myopia and a regular sampling matrix, the predicted

162    sampling density of the underlying mosaic for the highly myopic right eye is 8.05 cycles/mm (i.e.

163    9.50/1.18), closely approximating our measured value of 7.75 cycles/mm (see Fig. 3). In other

164    words, the sampling density of the myopic right eye was reduced by approximately the same ratio

165    as that predicted from the inter-eye MRI surface area data. It is likely that a clear reversal of

166    stimulus motion was not evident with right-eye viewing because the spatial resolution of the right

167    eye declined sharply for stimulus periodicities greater than 7.75 cycles/mm (Fig. 2).

168    Based on previously published work, we assume the underlying sampling matrix to be

169    retinal ganglion cells (see Introduction). Our results, therefore, are in accord with previous studies

170    reporting a decreased ganglion cell density in the peripheral retina of myopic observers.[1]

171

172    **CONCLUSIONS**

173    The spatial acuity (cycles/deg) of our observer's highly myopic right eye was almost half

174    that of his left, a reduction that cannot be explained solely by a linear areal expansion of the

175    underlying sampling units. While our data are consistent with evidence that myopic eyes have a

176    reduced peripheral resolution acuity relative to emmetropic eyes,[1,2] it remains an open question

177    as to why this is so. Assuming the enlarged receptive fields of the sampling units in a myopic eye

178    are a consequence of ocular stretching alone and not some compensatory dendritic growth

179    mechanism,[25] the reduced peripheral resolution evident in myopia may arise from: (i) increased

180    higher-order aberrations;[26,27] (ii) neuronal damage caused by retinal thinning;[28-30] (iii) aliasing

181    artefacts associated with neuronal undersampling;[1] and/or (iv) receptoral misalignment.[12,13] As

182    we have no new evidence with regard to optical quality or retinal thinning, we limit further

183    discussion here to the possible functional effects of undersampling and changes in receptor

184    orientation.

185        Several studies have reported that reduced neural sampling associated with myopia may

186    decrease peripheral visual performance.[1,3,31-33] However, our results suggest that the reduction in

187    sampling density in high myopia is no greater than would be expected from a simple linear

188    expansion of the retina. As such, the expanded optical image size should compensate for any

189    changes in sampling density. Functionally, therefore, myopia by itself should not result in any

190    additional sampling artefacts beyond what may already be present in the peripheral retina of an

191    emmetropic eye.

192        It is well established from human and animal studies that phototropic mechanisms actively

193    align photoreceptors towards a central area of the pupil to optimize light absorption.[34,35] However,

194    deviations in receptor alignment have been shown to be a consequence of axial elongation in

195    both human isomyopic[36] and anisometropic eyes.[37] The retinal image surface area of our

196    observer's highly myopic right eye was rotated almost 9⁰ anticlockwise from his left eye's image

197    surface (Fig. 1). The magnitude of this rotation may be sufficient to override local phototropic

198    forces,[37] leaving photoreceptors in the right eye aligned in a direction more or less perpendicular

199    to the outer shell of the eyeball.[38] This assumption could be tested in a future study by assessing

200    the directional properties of cone photoreceptors from psychophysical[36,37,39] or reflectometry[40]

201    measures of the Stiles–Crawford Effect of the First Kind, or from adaptive optics retinal imaging

202    systems.[35] Misalignment of the photoreceptors with the exit pupil would result in less efficient

203    luminance signal capture in the right eye, manifest as a reduction in contrast sensitivity for the

204    detection of visual targets. Accepting this, we conclude that changes in receptor orientation may

205    explain, at least in part, the large reduction in peripheral spatial acuity evident in the highly myopic

206    right eye of our observer. We speculate that if such misalignment causes sufficient visual

207    deprivation and/or disrupts local feedback processes through physiological stress, it may also

208    influence ocular growth and be a determining factor in the development of myopia itself.

209

210

211

212    **ARTICLE INFORMATION**

## REFERENCES

1. Chui TY, Yap MK, Chan HH, Thibos LN. Retinal Stretching Limits Peripheral Visual Acuity in Myopia. Vision Res 2005;45:593–605.

2. Ehsaei A., Chisholm CM, Pacey IE. Mallen EA. Visual Performance Fall-off with Eccentricity in Myopes Versus Emmetropes. J Optom 2013;6:36–44.

3. Wolsley CJ, Saunders KJ, Silvestri G, Anderson RS. Investigation of Changes in the Myopic Retina Using Multifocal Electroretinograms, Optical Coherence Tomography and Peripheral Resolution Acuity. Vision Res 2008;48:1554–61.

4. Thibos LN, Walsh DJ, Cheney FE. Vision Beyond the Resolution Limit: Aliasing in the Periphery. Vision Res 1987;27:2193-7.

5. Anderson SJ, Mullen KT, Hess RF. Human Peripheral Spatial Resolution for Achromatic and Chromatic Stimuli: Limits Imposed by Optical and Retinal Factors. J Physiol 1991;442:47–64.

6. Anderson RS, Wilkinson MO, Thibos LN. Psychophysical Localization of the Human Visual Streak. Optom Vis Sci 1992;69:171–4.

7. Anderson SJ, Drasdo N, Thompson CM. Parvocellular Neurons Limit Motion Acuity in Human Peripheral Vision. Proc Biol Sci 1995;26:129–38.

8. Sjöstrand J, Popovic Z, Conradi N, Marshall J. Morphometric Study of the Displacement of Retinal Ganglion Cells Subserving Cones Within the Human Fovea. Graefe's Arch Clin Exp Ophthalmol 1999;237:1014–23.

9. Atchison DA, Jones CE, Schmid KL, et al. Eye Shape in Emmetropia and Myopia. Invest Ophthalmol Vis Sci 2004;45:3380–6.

10. Atchison DA, Pritchard N, Schmid KL, et al. Shape of the Retinal Surface in Emmetropia and Myopia. Invest Ophthalmol Vis Sci 2005;46:2698–707.

11. Atchison DA, Thibos LN. Optical Models of the Human Eye. Clin Exp Optom 2016;99:99-106.

12. Enoch JM, Laties AM. An Analysis of Retinal Receptor Orientation. II. Predictions for Psychophysical Tests. Invest Ophthalmol 1971;10:959–70.

13. Choi SS, Enoch JM, Kono M. Evidence for Transient Forces/Strains at the Optic Nerve Head in Myopia: Repeated Measurements of the Stiles–Crawford Effect of the First Kind (SCE-I) Over Time. Ophthalmic Physiol Opt 2004;24:194-206.

14. Coletta NJ, Williams DR, Tiana CL. Consequences of Spatial Sampling for Human Motion Perception. Vision Res 1990;30:1631–48.

15. Galvin SJ, Williams DR, Coletta NJ. The Spatial Grain of Motion Perception in Human Peripheral Vision. Vision Res 1996;36:2283–95.

16. Wang YZ, Thibos LN, Bradley A. Undersampling Produces Non-Veridical Motion Perception, but not Necessarily Motion Reversal in Peripheral Vision. Vision Res 1996;36:1737-44.

17. Anderson SJ, Hess RF. Post-receptoral Undersampling in Normal Human Peripheral Vision. Vision Res 1990;30:1507–15.

18. Artal P, Derrington AM, Colombo E. Refraction, Aliasing, and the Absence of Motion Reversals in Peripheral Vision. Vision Res 1995;35:939–47.

19. Singh KD, Logan NS, Gilmartin B. Three-dimensional Modeling of the Human Eye Based on Magnetic Resonance Imaging. Invest Ophthalmol Vis Sci 2006;47:2272-9.

20. Gilmartin B, Nagra M, Logan N. Shape of the Posterior Vitreous Chamber in Human Emmetropia and Myopia. Invest Ophthalmol Vis Sci 2013;54:7240–51.

21. Nagra M, Gilmartin B, Logan NS. Estimation of Ocular Volume From Axial Length. Br J Ophthalmol 2014;98:1697–701.

22. Nagra M, Gilmartin B, Thai NJ, Logan NS. Determination of Retinal Surface Area.  J Anat. 2017;231:319-324.

23. Atchison DA, Markwell EL, Kasthurirangan S, et al. Age-related Changes in Optical and Biometric Characteristics of Emmetropic Eyes. J Vis 2008;8:29.1-20.

24. Richdale K, Bullimore MA, Sinnott LT, Zadnik K. The Effect of Age, Accommodation and Refractive Error on the Adult Human Eye. Optom Vis Sci 2016;93: 3–11.

25. Troilo D, Xiong M, Crowley JC, Finlay BL. Factors Controlling the Dendritic Arborization of Retinal Ganglion Cells. Vis Neurosci 1996;13:721–33.

26. Buehren T, Collins MJ, Carney LG. Near Work Induced Wavefront Aberrations in Myopia. Vision Res 2005;45:1297–312.

27. Collins MJ, Wildsoet CF, Atchison DA. Monochromatic Aberrations and Myopia. Vision Res 1995;35:1157–63.

28. Cheng SC, Lam CS, Yap MK. Retinal Thickness in Myopic and Non-Myopic Eyes. Ophthalmic Physiol Opt 2010;30:776–784.

29. Luo HD, Gazzard G, Fong A, et al. Myopia, Axial Length, and OCT Characteristics of the Macula in Singaporean Children. Invest Ophthalmol Vis Sci 2006;47:2773–81.

30. Lam DS, Leung KS, Mohamed S, et al. Regional Variations in the Relationship Between Macular Thickness Measurements and Myopia. Invest Ophthalmol Vis Sci 2007;48:376–82.

31. Strang N, Winn B, Bradley A. The Role of Neural and Optical Factors in Limiting Visual Resolution in Myopia. Vision Res 1998;38:1713–21.

32. Vera-Diaz FA, McGraw PV, Strang NC, Whitaker D. A Psychophysical Investigation of Ocular Expansion in Human Eyes. Invest Ophthalmol Vis Sci 2005;46:758-63.

33. Atchison DA, Schmid KL, Pritchard N. Neural and Optical Limits to Visual Performance in Myopia. Vision Res 2006;46:3707–22.

34. Roorda A, Williams DR. Optical Fiber Properties of Individual Human Cones. J Vis 2002;2:404–12.

35. Walker MK, Blanco L, Kivlin R, et al. Measurement of the Photoreceptor Pointing in the Living Chick Eye. Vision Res 2015;109:59–67.

36. Choi SS, Garner LF, Enoch JM. Stiles-Crawford Effect of the First Kind (SCE-I) in Post-Photorefractive Keratectomy and Anisometropic Subjects. Ophthalmic Physiol Opt 2003;23:473–6.

37. Choi SS, Garner LF, Enoch JM. The Relationship Between the Stiles-Crawford Effect of the First Kind (SCE-I) and Myopia. Ophthalmic Physiol Opt 2003;23:465–72.

38. Enoch J M, Choi SS, Kono M, et al. Receptor Alignments and Visual Fields in High and Low Myopia. In Wall M, Mills RP, eds. Perimetry Update 2000/2001. The Netherlands: Kugler Publications; 2001:373-87.

39. Westheimer G. Directional Sensitivity of the Retina: 75 Years of Stiles–Crawford Effect. Proc Biol Sci 2008;275:2777–86.

40. Gao W, Cense B, Zhang Y, et al. Measuring Retinal Contributions to the Optical Stiles–Crawford Effect with Optical Coherence Tomography. Opt Express, 2008;16:6486–501.

**FIGURE LEGENDS**

**Figure 1: 3D Magnetic Resonance Ocular Images.**  (A) 3-dimensional MRI co-ordinates for nasal and temporal quadrants were, for both RE and LE of the observer, collapsed and superimposed about the nasal-temporal meridian and plotted (as a 10-point moving average) in 2-dimensions as distance-along and distance-from the visual axis for approximately 15 to 100% of eye length. The axial lengths of the right and left eye were 27.9 mm and 21.9 mm, respectively. The variance in distance from the axis for a given distance along the axis designates the degree of irregularity in retinal shape occurring across the nasal and temporal quadrants. Thus, relative to the LE, the variation in retinal shape in the temporal quadrant is substantially greater in the highly myopic RE.  (B) The position of NP2 was used to locate, by projection, the regions of the temporal retinae conjugate with the 40º nasal location of the stimulus display. As the difference in positions of NP2 for the RE and LE was small, single lines were drawn at 40º and at 40°±3º to represent, for both eyes, the angular subtense of the stimulus display. BC and FG (mm) indicate the distances projected onto the temporal retinae of RE and LE by the stimulus display and were assumed to be linear. BC and FG were used to calculate the inter-eye ratio of retinal image surface areas. (C and D) Visualization of the generated 3-dimensional eye surfaces, pseudo-coloured with reference to the axial distance from the corneal pole.
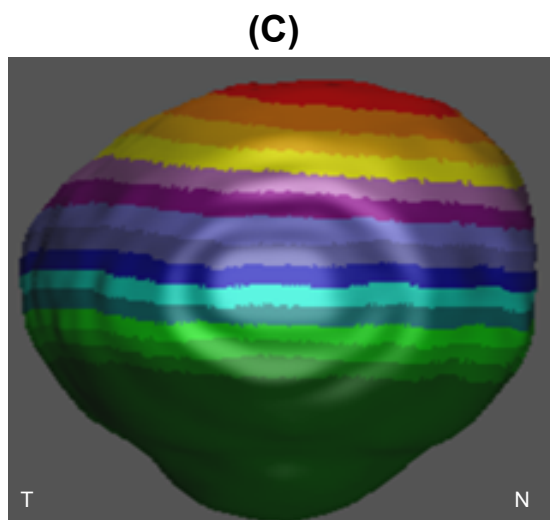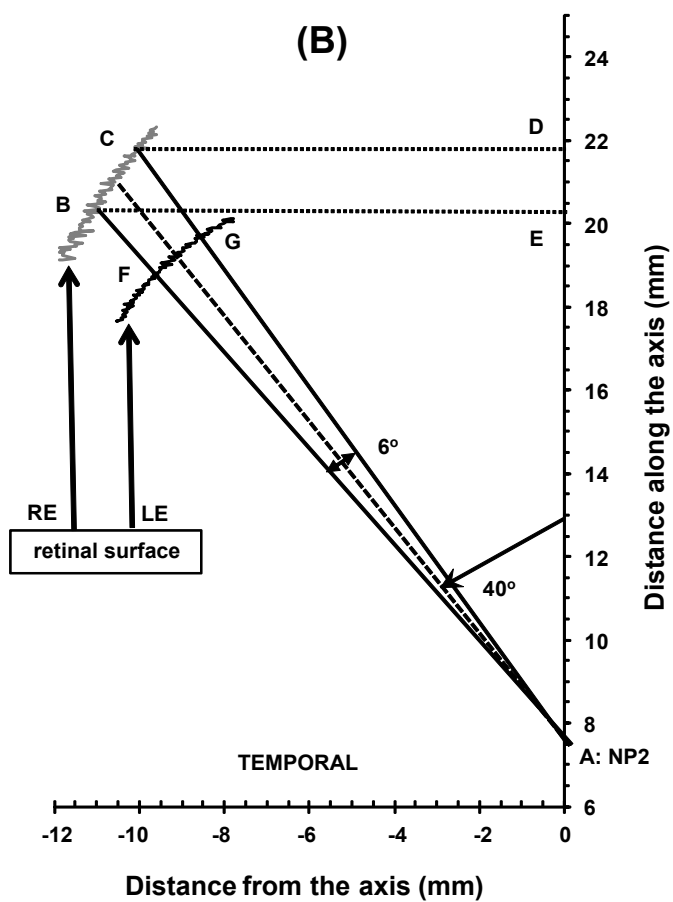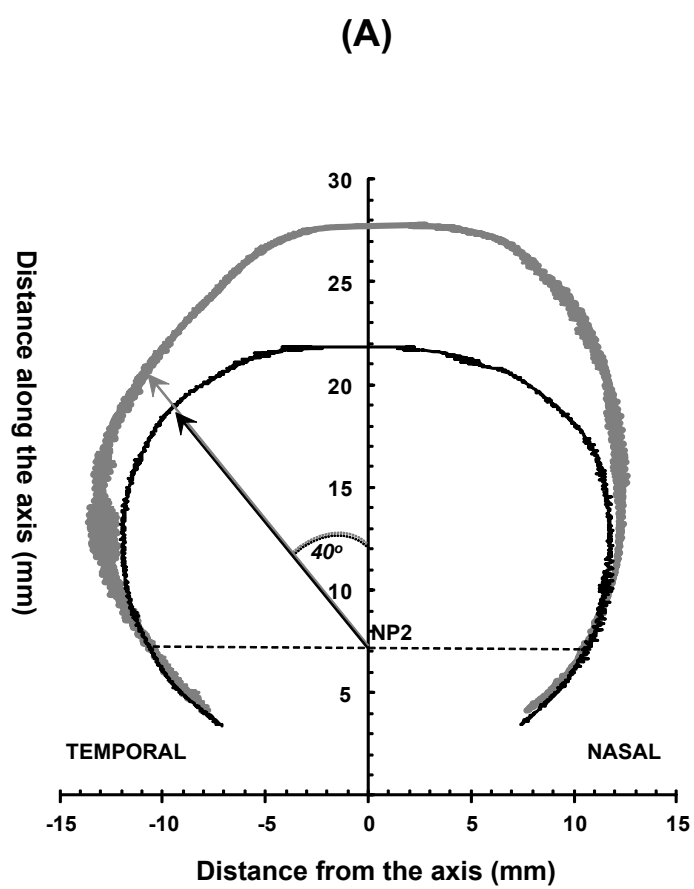
**Figure 2: Visual Performance for Detection of Sinusoidal Gratings.** Performance (% of correct responses) of the observer for the detection of sinusoidal gratings drifting at 8 Hz, plotted as a function of grating spatial frequency in cycles/mm (open circles, left eye; closed circles, right eye). The results are for horizontal gratings of 80% contrast, positioned 40º in the temporal retina. The upper (and lower) 95% confidence limit was ≤ three times the symbol size. The curve through each data set is the least-squares fit of a Weibull function, and the solid horizontal lines show the criterion level for determining spatial acuity (80% correct) and chance performance (50% correct).

Spatial acuity for the left eye was 16.46 cycles/mm (4.25 cycles/deg); acuity for the right eye was 7.78 cycles/mm (2.38 cycles/deg).
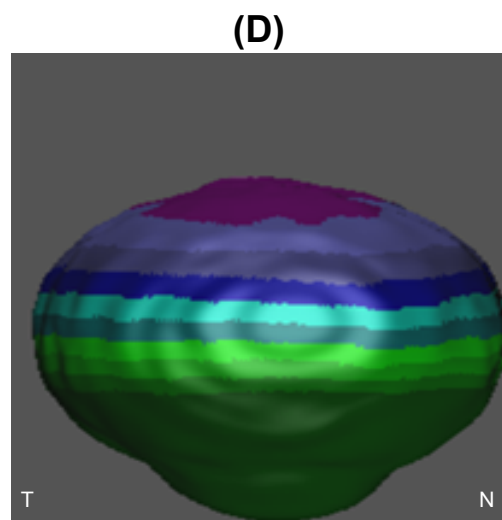
**Figure 3: Visual Performance for Direction Discrimination of Sinusoidal Gratings.** Performance (% of correct responses) of the observer for the direction discrimination of sinusoidal gratings drifting at 8 Hz, plotted as a function of grating spatial frequency in cycles/mm (open circles, left eye; closed circles, right eye).  The results are for horizontal gratings of 80% contrast, positioned 40⁰ in the temporal retina. The upper (and lower) 95% confidence limit was ≤ three time the symbol size. The curve through each data set is the least-squares fit of a Weibull function down to the first datum below chance performance (50% correct), with a simple line fit to the remaining data. Note that the direction discrimination function falls to chance at 9.50 cycles/mm (2.45 cycles/deg) for the left eye and 7.75 cycles/mm (2.37 cycles/deg) for the right eye.

Figure 1



**(A)**

Distance along the axis (mm)

30

25

20

15

40°

10

NP2

5

TEMPORAL                    NASAL

-15    -10    -5    0    5    10    15

Distance from the axis (mm)

**(B)**

24

C                                        D    22

B                                             20    E

G

F

6°

RE        LE

retinal surface

40°

Distance along the axis (mm)

TEMPORAL                                    A: NP2

-12    -10    -8    -6    -4    -2    0

18

16

14

12

10

8

6

Distance from the axis (mm)

**(C)**

T                    N

**Right eye**

**(D)**

T                    N

**Left eye**

Figure 2

# Detection functions



LE: -2.25/-1.00 x 27
central VA = 6/5

RE: -19.75/-1.50 x 95
central VA = 6/6

**Proportion correct**

**Spatial frequency (cycles/mm)**

Figure 3

**Discrimination functions**



LE: -2.25/-1.00 x 27
central VA = 6/5

RE: -19.75/-1.50 x 95
central VA = 6/6